Spectroscopy and shell model calculations in Si isotopes

S. S. Bhattacharjee, R. Bhattacharjee, R. Raut, S. S. Ghugre, A. K. Sinha, L. Chaturvedi, T. Trivedi, U. Garg, S. Ray, B. K. Yogi, M. Kumar Raju, R. Chakrabarti, S. Mukhopadhyay, A. Dhal, R. P. Singh, N. Madhavan, S. Muralithar, S. Saha, J. Sethi, and R. Palit

Phys. Rev. C **91**, 044306 — Published 7 April 2015

DOI: 10.1103/PhysRevC.91.044306

Spectroscopy and Shell Model Calculations in Si Isotopes

S. S. Bhattacharjee, R. Bhattacharjee, R. Raut,* S. S. Ghugre, and A. K. Sinha
UGC-DAE Consortium for Scientific Research, Kolkata Centre, Kolkata 700098, India

L. Chaturvedi and T. Trivedi
Guru Ghasidas University, Bilaspur 495009, India

U. Garg
Department of Physics, University of Notre Dame, Notre Dame, Indiana 46556, USA

S. Ray
Amity Institute of Nuclear Science and Technology, Amity University, Noida, Uttar Pradesh 201303, India

B. K. Yogi
Department of Physics, Government College, Kota 324009, India

M. Kumar Raju
Nuclear Physics Department, Andhra University, Visakhapatnam 530003, India

R. Chakrabarti and S. Mukhopadhyay
Nuclear Physics Division, Bhabha Atomic Research Centre, Mumbai 400085, India

A. Dhal, R. P. Singh, N. Madhavan, and S. Muralithar
Inter University Accelerator Centre, Aruna Asaf Ali Marg, New Delhi 110067, India

S. Saha, J. Sethi, and R. Palit
Tata Institute of Fundamental Research, Mumbai 400005, India

(Dated: March 13, 2015)

The ^{29}Si nucleus has been studied using heavy-ion induced fusion-evaporation reaction and, for the first time, using a large array of high resolution γ-ray detectors. High spin states of the nucleus have been populated using ^{18}O(^{16}O,αn) and ^{18}O(^{13}C,$2n$) reactions at E_{lab} = 30-34 MeV. Previously reported levels have been confirmed and a new level has been identified in the present study. Spin-parity assignments have been carried out based on the anisotropy and polarization measurements of the observed γ-transitions. Level lifetimes have been measured using Doppler Shift Attenuation Method (DSAM), with modified analysis techniques for the thick molecular target (Ta_2O_5) used in the present setup. Lifetime of the lowest negative parity state at E_x = 3624 keV has been substantially modified from the previously reported value. Large basis shell model calculations have been carried out for the nucleus using updated interactions and the results corroborate the experimental findings. The calculations have also been carried out for the neighbouring ^{28,30}Si isotopes. In case of the ^{28}Si nucleus, the calculations adequately reproduce most of the deformed structures, as represented by the quadrupole moments extracted therefrom. In the ^{30}Si nucleus, the negative parity states have been reproduced for the first time without any ad hoc lowering of the single particle energies. It can be generally stated that the shell model calculations adequately describe the experimental observations in these nuclei.

PACS numbers: 23.20.Lv,21.10.Hw,21.60.Cs

I. INTRODUCTION

The *sdpf* nuclei, with $Z \sim$ 12-16 and $N \sim$ 14-18, have been subjects of recent spectroscopic investigations, carried out using contemporary facilities [1–4]. The primary motivation has been to probe the evolving structure of these nuclei belonging to the transitional region between the line of stability and the island of inversion [5, 6]. A preferential occupation of the fp-shell configurations even at lower excitation energies and the development of collectivity based on pure *sd* configurations is indicated for these nuclei. The associated theoretical studies have also been zealously pursued in conjunction with the experimental endeavours, particularly within the purview

*Electronic address: rraut@alpha.iuc.res.in

of the nuclear shell model. Shell model calculations in this region have resorted to adhoc adjustments [7] in the single particle energies while calculations with updated interactions [8] and reasonable configuration space have indicated such modifications to be inessential [9].

Most of the information on the level structure of these nuclei is based on experimental investigations carried out with modest detector setups and light-ion beams. The results from these measurements, for instance the level lifetimes and the γ-ray angular distributions, exhibit substantial scatter even at low excitation energies and spins. The ambiguities and/or uncertainties in the experimental findings can be found, for example, in the ^{29}Si ($Z = 14, N = 15$) nucleus, being probed in the present study, as illustrated in Fig. 1. The lifetime of the 1274 keV ($J^\pi = 3/2^+$) level has been reported in several previous studies [10–18] but the values are considerably variant, with a few of them having substantial uncertainties. Similarly, the multipolarity and the electromagnetic assignment of the 1596 keV transition, de-exciting the lowest negative parity state (3624 keV, $J^\pi = 7/2^-$), has been investigated in a previous study [19] carried out with a NaI(Tl) scintillator detector, with the concomitant large uncertainties on the angular distribution coefficients (Fig. 1). This is a less than optimal situation since the negative parity levels in the *sdpf* nuclei are of particular significance as they originate from cross-shell excitations. Unambiguous identification of these levels along with the related information (lifetime, de-exciting transitions, multipolarity, electromagnetic nature, mixing ratio) is pertinent for benchmarking model calculations. In particular, probing the lowest negative parity level in these nuclei may provide an indication to the *sd-fp* shell gap and requires determination of the associated measurables.

The present work reports the investigation of the level structure of ^{29}Si, populated through heavy-ion induced fusion-evaporation reaction, using a large array of high resolution composite γ-ray detectors which also facilitate polarization measurements. The results have been compared with shell model calculations using updated interactions and larger model spaces and are found to be in close agreement. The large basis shell model calculations, have been extended to the neighbouring ^{28,30}Si nuclei [7, 20] for a comparative interpretation. The calculations for ^{28}Si could satisfactory reproduce the deformed states reported previously by Jenkins *et al.* [20]. Further, the predicted negative parity states in ^{30}Si, are in reasonable agreement with the observed level sequences. Interestingly, the calculations did not require any system dependent lowering of the single-particle energies of the $f_{7/2}$ and the $p_{3/2}$ orbitals as was found necessary in the previous studies [7, 21, 22].

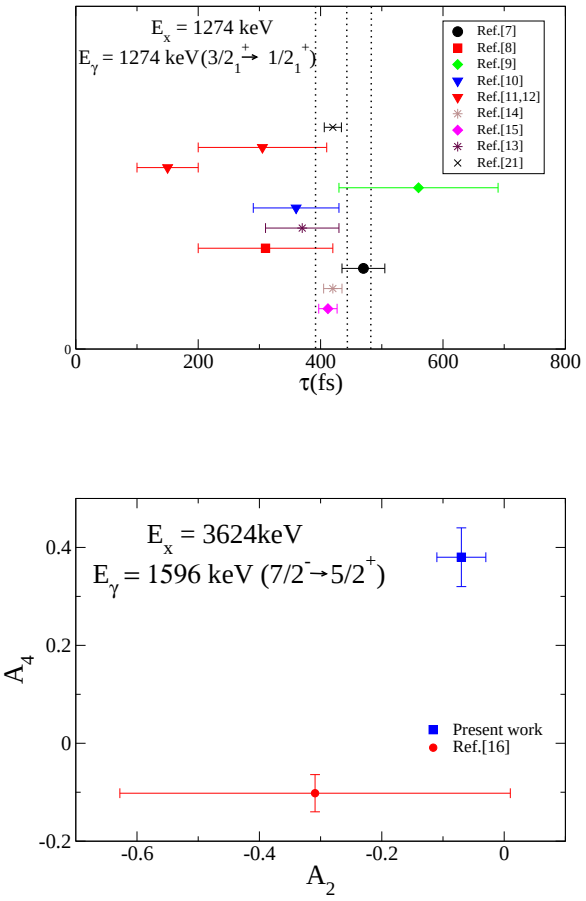

FIG. 1: (Color online) (Upper panel) The level lifetimes of the 1274 keV ($J^\pi = 3/2^+$) state in the ^{29}Si nucleus from earlier measurements. The results from the present measurement are also included (see text for details). (Bottom panel) Angular distribution coefficients for the 1596 keV ($7/2^- \rightarrow 5/2^+$) transition in the ^{29}Si nucleus from the earlier and the present work (see text for details)

II. EXPERIMENTAL DETAILS AND DATA ANALYSIS

High spin states in ^{29}Si have been populated using the ^{18}O(^{16}O, αn) and ^{18}O(^{13}C, $2n$) reactions at incident beam energies of 34 and 30 MeV, delivered by the pelletron facilities at Inter University Accelerator Center (IUAC), New Delhi and Tata Institute of Fundamental Research (TIFR), Mumbai, respectively. The multi-Clover detector array, the Indian National Gamma Array (INGA) has been used to detect the de-exciting γ-rays. The details of the experimental setup are outlined in Refs. [1, 3]. Two and higher fold coincidence events have been recorded and subjected to a detailed offline analysis.

The energy calibration has been carried out using the radioactive sources as well as the beam-off radioactivity

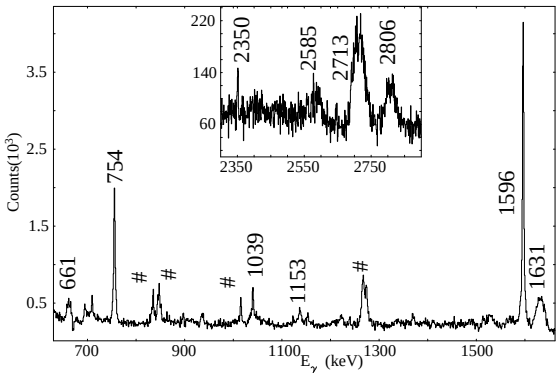

FIG. 2: Coincidence spectrum with gates on the 1274 keV and the 2028 keV transitions in ^{29}Si. The transitions belonging to the ^{29}Si nucleus are labelled with the respective energies while the contaminant peaks are identified with #. The inset illustrates the higher energy transitions ($E_\gamma > 2.0 MeV$).

data, which provided for the calibration points at higher γ-ray energies. Most of the transitions belonging to ^{29}Si exhibited Doppler effects (shifts and shapes depending on the level lifetimes). Hence, the data have been sorted to form angle dependent $E_\gamma - E_\gamma$ matrices with the 90° detectors on one axis and the detectors at one of the remaining angles on the other axis for subsequent analysis. Fig. 2, depicts the (coincident) transitions observed at 90° with gates on the 1274 keV ($3/2^+ \rightarrow 1/2^+$) and the 2028 keV ($5/2^+ \rightarrow 1/2^+$) transitions in the ^{29}Si nucleus.

The observations of substantial Doppler shapes did not permit us to undertake the conventional measurement of the ratio for Directional Correlation from Oriented nuclei (DCO) for multipolarity assignments of the observed γ-ray transitions [1, 2] . The dominant multipolarity of the observed transitions has thus been determined using the anisotropy ratio ($R_{anisotropy}$) [2, 3], defined as,

$$R_{anisotropy} = \frac{I_{\gamma_1}\ (at\ \theta_1\ gated\ by\ \gamma_2\ at\ 90°)}{I_{\gamma_1}\ (at\ \theta_2\ gated\ by\ \gamma_2\ at\ 90°)} \quad (1)$$

As presented in Fig. 3, this method facilitates distinction between transitions of different multipolarities. For the present detector geometry, gate on a pure dipole transition would lead to $R_{anisotropy} = 1.9$ for pure quadrupole transition and $R_{anisotropy} = 1.0$ for pure dipole transition. In case of gate on pure quadrupole transition, $R_{anisotropy} = 1.7$ for a pure quadrupole transition and $R_{anisotropy} = 1.0$ for pure dipole transition. These values have been extracted using transitions of known multipolarities from different nuclei populated in the same experiment. The $R_{anisotropy}$ information together with the linear polarization measurements enable the spin-parity assignments for the observed

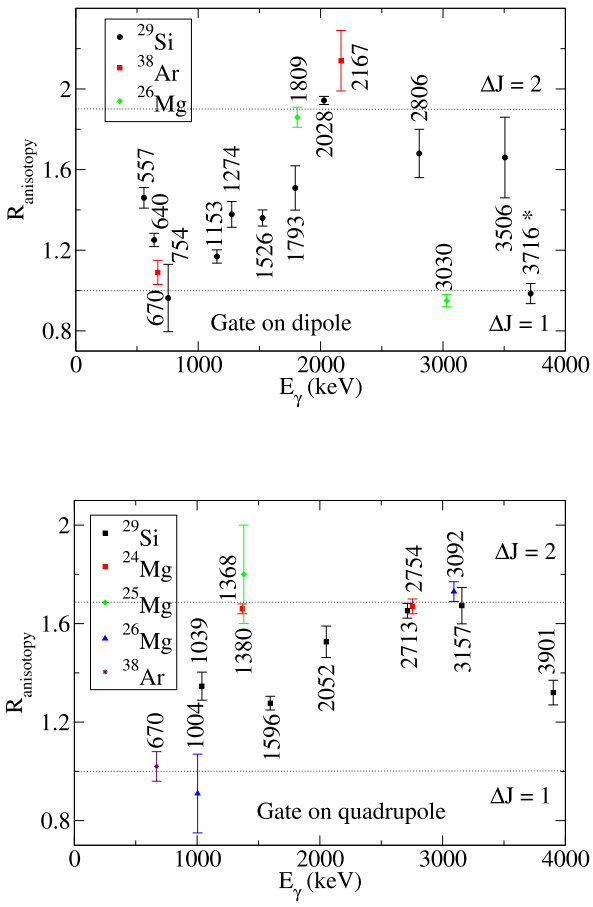

FIG. 3: (Color online) The experimental $R_{anisotropy}$ values for transitions in ^{29}Si from the present work. The new transition is labelled with *.

levels.

The Clover detector has four identical crystals in a close packed geometry, with minimal dead-layer / spacing in-between the crystals. This geometry can be applied for linear polarization measurements of the observed γ-ray transitions with any of the four crystals as the scatterer and the two adjacent crystals, which correspond to mutually perpendicular directions, as the absorbers. The preferential scattering of electric and magnetic transitions respectively in the direction perpendicular and parallel to the reaction plane, allows us to identify the electromagnetic nature of the transition. Since intensity is proportional to the differential cross section of Compton scattering, the intensities of the mutually perpendicular Compton scattered γ-rays, denoted by $N_\perp$ and $N_\parallel$, are used to obtain a polarization asymmetry, Δ_{Pol} defined as,

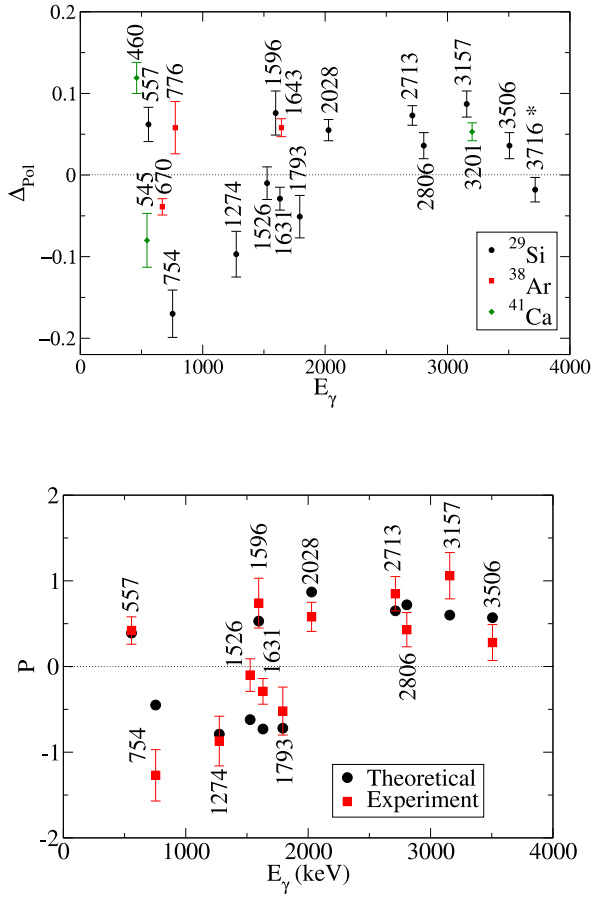

FIG. 4: (Color online) Plot of polarization asymmetry for transitions in ^{29}Si from the present measurements (upper panel). Transitions with established electromagnetic nature in ^{41}Ca and ^{38}Ar have been included for reference. These nuclei have been populated following the interaction of the beam halo with the aluminum target frame. The corresponding polarization (P) values have been also plotted (lower panel). The new transition identified in the present work has been labelled with *.

$$\Delta_{Pol} = \frac{aN_\perp - N_\parallel}{aN_\perp + N_\parallel}, \qquad (2)$$

The geometrical effects of the array have to be incorporated in the estimation of the polarization asymmetry. This is represented by the asymmetry term, a, obtained from the ratio of $N_\parallel$ to $N_\perp$ for γ-rays from radioactive sources which are characteristically unpolarized. This constant was obtained in the previous studies carried out using the same detector setups [2, 3] and has been used for the present measurements. Fig. 4 illustrates the polarization asymmetry for the transitions in ^{29}Si along with those for transitions of known electromagnetic nature from ^{38}Ar and ^{41}Ca nuclei, included here for reference. From the experimental asymmetry, the polarization ($P = \Delta_{Pol}/Q$, Q being the polarization sensitivity) has been obtained for the transitions, using the method detailed in Ref. [3], and are presented in Fig. 4. The theoretical polarization for these transitions, using the known mixing ratios from the previous studies [23], have also been calculated and included in the plot (Fig. 4). The agreement of the theoretical polarization with the experimental values is satisfactory.

The observation of Doppler shapes / shifts in the present work facilitated the determination of level lifetimes using the Doppler shift attenuation method (DSAM). The analysis of the shapes / shifts has been carried out using the LINESHAPE [24] package modified for DSAM with a thick molecular target, as detailed in Ref. [9]. The slowing down of the residue of interest in the thick Ta_2O_5 target has been simulated using the stopping powers calculated using the SRIM [25] software. The cross section for the production of the residues along the thickness of the target, with evolving beam energy, has been obtained from the statistical model calculations using the PACE4 [26] code. The results of the analysis are summarized in the subsequent section.

III. RESULTS

The level scheme of the ^{29}Si nucleus, following the present study, is illustrated in Fig. 5. Table I records the level energies, the de-exciting γ-ray transitions and the spin-parity assignments. Most of the levels and the transitions in ^{29}Si, reported in the previous studies, have been confirmed in the present investigation with high resolution spectroscopic tools in the form of large array of Compton suppressed Clover detectors. In addition, a new level at E_x = 7340 keV de-exciting by 3716 keV γ-ray transition has been identified in this work.

The 1631 keV transition de-exciting the 5255 keV ($9/2^-$) level is noteworthy. This transition has been addressed in the previous studies, especially by Bardin *et al.* [27, 28] to explore the development of collectivity in the nucleus. The negative parity sequence was identified as a possible candidate for a rotational structure. The angular distribution for the 1631 keV γ-ray was carried out and the transition was identified to have a quadrupole-dipole (mixed) multipolarity with a substantial mixing (δ = -0.43, [23]). Owing to the high mixing ratio of the transition, the dominant multipolarity could not be ascertained from the present anisotropy measurements. However, such high mixing ratio leads to the possibility of this transition having either a M1+E2 or an E2+M3 nature. An unambiguous conclusion based solely on the angular distribution measurement is difficult. Nevertheless, if we consider the theoretical polarization in comparison to the experimental value, these two possibilities produce widely different results. While the M1+E2 option results in a theoretical polarization of -0.7, in reasonable agreement

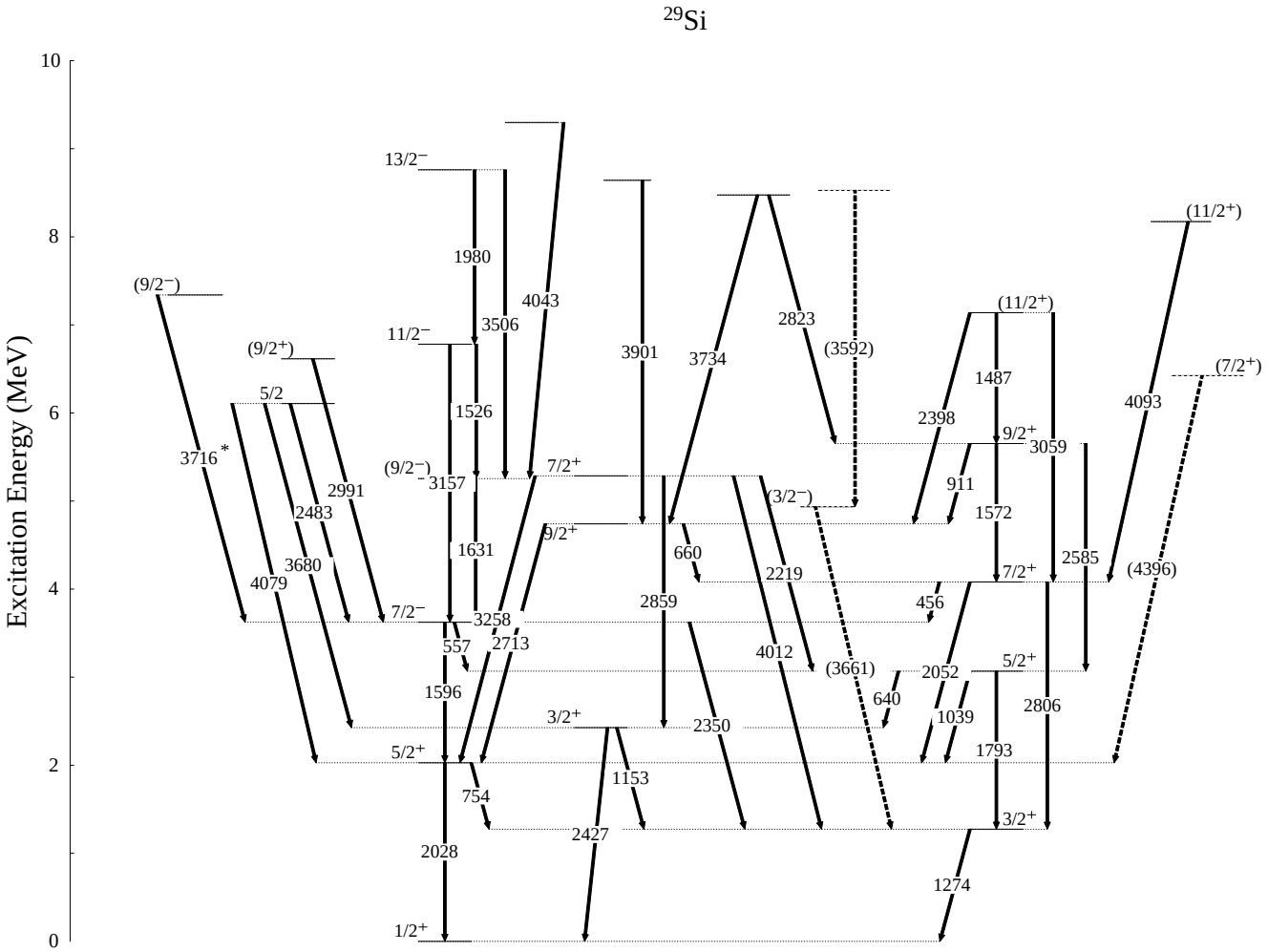

FIG. 5: The level scheme of the ^{29}Si nucleus from the present work. The new level and the de-exciting transition has been labeled with *. The levels and the transitions that are known from the previous studies but could not be conclusively confirmed in the present work have been indicated with dotted lines.

with the experimental value (-0.3±0.1), the E2+M3 possibility produces a theoretical polarization value of +0.8 that is widely discrepant with respect to the measurements. The possibility of the transition being M1+E2 is further corroborated by the lifetime of the 5255 keV level, that was previously reported to be 118 fs and has been confirmed in the present work. The alternative E2+M3 mixed character would indicate a highly retarded transition with a much longer lifetime.

The 1596 keV transition de-exciting the 3624 keV $(7/2^-)$ level [23] is also noteworthy. This transition has previously been studied by Becker *et al.* [19] and was assigned a mixed dipole-quadrupole character, though with a high uncertainty on the mixing ratio ($\delta = 0.02 \pm 0.02$). The transition is significant owing to the associated change in parity and the long ($\sim$ 3.8 ps) level lifetime (compared to neighbouring states). This is indicative of a change in the structure therein. Indeed, the 3624 keV $(7/2^-)$ level has been interpreted as the band-head of the $K^\pi = 7/2^-$ band in the previous studies [10, 28]. Such a scenario warrants a re-examination of the 1596 keV transition with the contemporary spectroscopy tools, as used in the present investigation. The $R_{anisotropy}$ value for the transition, from the present measurement, is 1.27 $\pm$ 0.03 in a quadrupole gate, indicating a dominant dipole nature with quadrupole admixture, while the value of polarization asymmetry (0.08 $\pm$ 0.03) is suggestive of a principally electric behaviour. In the light of these results, the 1596 keV has been interpreted as a mixed E1+M2 transition in the present work. The mixing ratio of 0.14 $\pm$ 0.04 has been estimated from the angular distribution analysis of the 1596 keV γ-ray, following the prescription detailed in Ref. [3]. The fit to the angular distribution from the current study and the plot for the corresponding χ^2 is illustrated in Fig. 6. The theoretical polarization (P) for the transition, calculated using this mixing ratio, is in reasonable agreement with the experimental result. It is interesting to note a similar feature in the neighbouring ^{31}Si isotope wherein

TABLE I: Details of γ-ray transitions of the ^{29}Si nucleus, observed in the present work.

$E_i^b(keV)$	$E_\gamma^a(keV)$	$E_f^b(keV)$	Br(%)	J_i^π	J_f^π	$R_{anisotropy}$	Δ_{Pol}	Assignment
1274	1273.8±0.4	0	100	$3/2_1^+$	$1/2_1^+$	1.37±0.06^D	-0.097±0.028	M1+E2
2028	754.2±0.4	1274	7.94±0.10	$5/2_1^+$	$3/2_1^+$	0.96±0.17^D	-0.170±0.029	M1+E2
	2027.6±0.5	0	92.06±0.60	$5/2_1^+$	$1/2_1^+$	1.94±0.02^D	0.055±0.013	E2
2427	1152.6±0.8	1274		$3/2_2^+$	$3/2_1^+$	1.17±0.03^D		D+Q
	2427.0 ±2.0	0		$3/2_2^+$	$1/2_1^+$			M1+E2^N
3067	640.0±0.6	2427	0.42±0.05	$5/2_2^+$	$3/2_2^+$			
	1038.8±0.3	2028	16.03±0.36	$5/2_2^+$	$5/2_1^+$	1.35±0.06^Q		M1+E2^N
	1792.6±0.2	1274	83.55±1.03	$5/2_2^+$	$3/2_1^+$	1.51±0.11^D	-0.051±0.026	M1+E2
3624	556.7±0.2	3067	11.23±0.46	$7/2_1^-$	$5/2_2^+$	1.46±0.05^D	0.062±0.021	E1+M2
	1595.9±0.4	2028	86.57±1.70	$7/2_1^-$	$5/2_1^+$	1.27±0.03^Q	0.076±0.027	E1+M2
	2349.6±0.4	1274	2.19±0.18	$7/2_1^-$	$3/2_1^+$			
4080	456.4±0.5	3624	< 1.00	$7/2_1^+$	$7/2_1^-$			
	2051.9±0.8	2028	32.00±10.00	$7/2_1^+$	$5/2_1^+$	1.52±0.06^Q		M1+E2^N
	2806.0±2.0	1274	67.00±18.00	$7/2_1^+$	$3/2_1^+$	1.68±0.12^D	0.036±0.016	E2
4741	660.6±0.6	4080	6.00±5.00	$9/2_1^+$	$7/2_1^+$			
	2713.0±2.0	2028	93.00±7.00	$9/2_1^+$	$5/2_1^+$	1.65±0.03^Q	0.073±0.012	E2
4935	3661.0±2.0	1274	100	$(3/2_1^-)$	$3/2_1^+$			
5255	1631.5±0.4	3624	100	$(9/2_1^-)$	$7/2_1^-$		-0.029±0.014	(M1+E2)^N
5286	2219.0±2.0	3067		$7/2_2^+$	$5/2_2^+$			
	2859.0±2.0	2427		$7/2_2^+$	$3/2_2^+$			
	3258.0±2.0	2028		$7/2_2^+$	$5/2_1^+$			M1+E2^N
	4012.0±2.0	1274		$7/2_2^+$	$3/2_1^+$			
5652	911.5±0.3	4741		$9/2_2^+$	$9/2_1^+$			
	1572.0±2.0	4080		$9/2_2^+$	$7/2_1^+$			M1+E2^N
	2585.0±2.0	3067		$9/2_2^+$	$5/2_2^+$			
6107	2483.0±2.0	3624		5/2	$7/2_1^-$			
	3680.0±2.0	2427		5/2	$3/2_2^+$			
	4079.0±2.0	2028		5/2	$5/2_1^+$			D+Q^N
6424	4396.0±2.0	2028	100	$(7/2_3^+)$	$5/2_1^+$			D+Q^N
6615	2991.0±2.0	3624	100	$(9/2_3^+)$	$7/2_1^-$			
6781	1526.4±0.6	5255	45.00±17.00	$11/2_1^-$	$(9/2_1^-)$	1.36±0.04^D	-0.01±0.02	M1+E2
	3157.0±2.0	3624	54.00±28.00	$11/2_1^-$	$7/2_1^-$	1.67±0.07^Q	0.087±0.016	E2
7139	1487.0±2.0	5652		$(11/2_1^+)$	$9/2_2^+$			(M1+E2)^N
	2398.0±2.0	4741		$(11/2_1^+)$	$9/2_1^+$			
	3059.0±2.0	4080		$(11/2_1^+)$	$7/2_1^+$			
7340	3716.0±2.0	3624	100	$9/2_2^-$	$7/2_1^-$	0.98±0.05^D	-0.018±0.015	(M1+E2)
8173	4093.0±2.0	4080	100	$(11/2_2^+)$	$7/2_1^+$			
8475	2823.0±2.0	5652			$9/2_2^+$			
	3734.0±2.0	4741			$9/2_1^+$			
8527	3592.0±2.0	4935	100		$3/2_1^-$			
8642	3901.0±2.0	4741	100		$9/2_1^+$	1.32±0.05^Q		D+Q
8761	1980.0±2.0	6781		$13/2_1^-$	$11/2_1^-$			
	3506.0±2.0	5255		$13/2_1^-$	$(9/2_1^-)$	1.66±0.20^D	0.036±0.016	E2
9298	4043.0±2.0	5255	100		$(9/2_1^-)$			

^{Q} From quadrupole gate. ^{D} From dipole gate. ^{N} Adopted from NNDC.

*

an E1+M2 transition (1438 keV), with $\delta = 0.11 \pm 0.01$, de-excites the lowest negative parity state at 3133 keV ($7/2^-$). However, the experimental B(E1) value for the 1596 keV (^{29}Si) transition is $\sim 8{\times}10^{-5}$ Wu while that for the 1438 keV transition (^{31}Si) is $\sim 61{\times}10^{-5}$ Wu, which could possibly indicate an enhancement in the collectivity with increasing neutron number in the Si isotopes.

As already mentioned in the preceding discussions, observation of Doppler shapes / shifts in the γ-transition peaks of ^{29}Si, enabled extraction of the corresponding level lifetimes using the DSAM technique. The modified LINESHAPE package [9] has been used for the purpose.

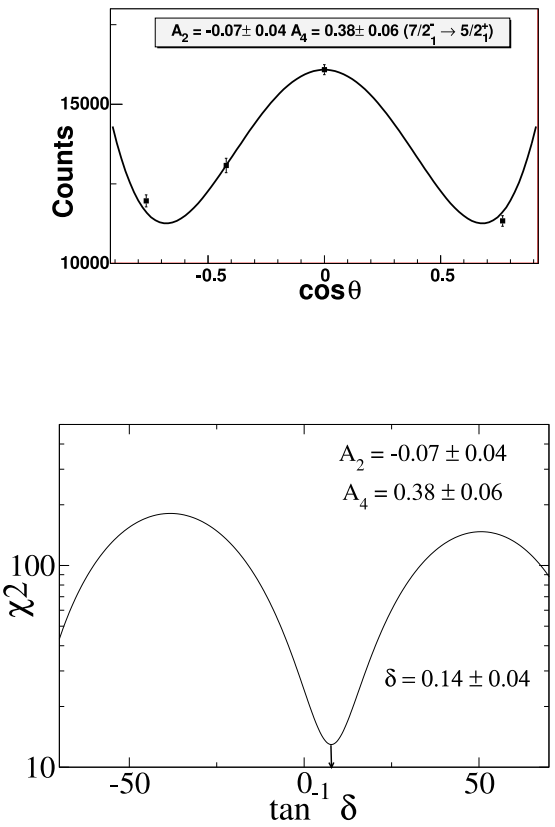

FIG. 6: (Color online) The angular distribution fit for the 1596 keV ($7/2_1^- \rightarrow 5/2_1^+$) transition in the ^{29}Si nucleus and the corresponding χ^2 analysis for obtaining the mixing ratio.

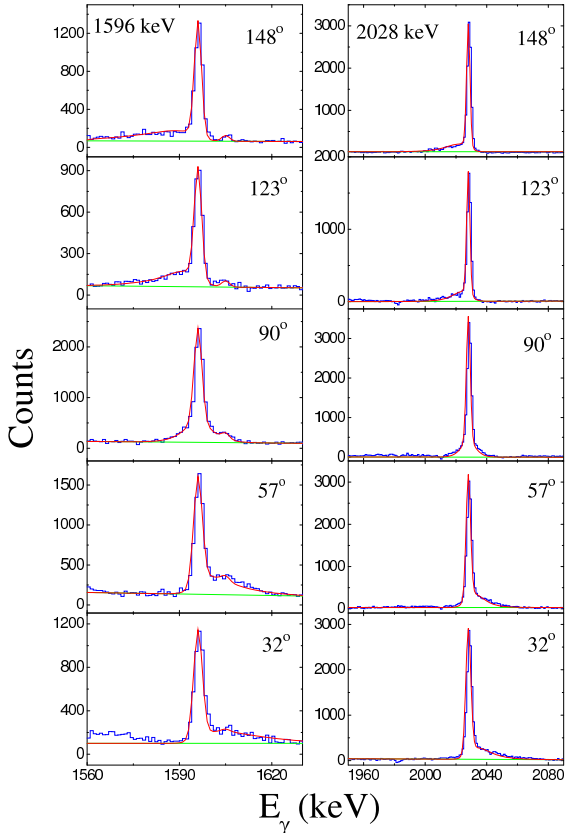

FIG. 7: (Color online) Representative fits to the Doppler shapes observed for the 1596 keV and the 2028 keV transitions in ^{29}Si nucleus.

Least square fitting of the observed shapes to the calculated ones have been carried out simultaneously at five different angles, 148°, 123°, 90°, 57°, 32°, for determination of the level lifetimes. The parameters for the fitting procedure included the level lifetime, the side-feeding time, the peak height, the contaminant peak(s) and the background parameters. The results of the lifetime analysis in case of ^{29}Si are recorded in Table II while Fig. 7 illustrates representative fits to the Doppler shapes for the 1596 keV and the 2028 keV transitions. Level lifetimes that could be extracted from gates on transitions above (GTA) have been quoted as definite values while those that could be analyzed only with gates on transitions below (GTB) have been stated as the upper limits, after incorporating the side feeding contribution. The dominant uncertainties on the quoted lifetimes stem from the uncertainties in the stopping power estimates that are typically $\sim$ 10%. Thus, the stopping powers have been varied by 10% and the resulting dispersions in the level lifetimes have been included in the quoted uncertainties. Most of the level lifetimes / limits derived in the present study are in agreement with the previously reported values [23]. However, the level lifetime for $E_x = 3624$ keV, de-excited by the 1596 keV transition, has been determined to be $\tau = 2.5 \pm 0.2$ in the present work, and is at variance with the previously reported value of $\tau = 3.8 \pm 0.1$. This being the lowest negative parity state, accurate estimation of the level and the transition properties can contribute to refining the model calculations, through their impact on the *sd-pf* shell gap and the transition probabilities. Upper limit on the lifetime has also been obtained for the $E_x = 7340$ keV level, de-exciting by the 3716 keV transition, that has been reported for the first time in the present work.

IV. SHELL MODEL CALCULATIONS

Large basis shell model calculations have been carried out for the ^{29}Si nucleus and the neighbouring ^{28,30}Si isotopes using the shell model code NuShellX@MSU [29]. The *USDA* [8] and the *SDPFMW* [1, 30] interactions have been used. The basis space used was either *sd*, consisting of the $d_{3/2}$, $s_{1/2}$ and $d_{5/2}$ orbitals, or the *sdpf*, consisting of the *sd* and the $f_{7/2}$, $p_{3/2}$, $p_{1/2}$ and $f_{5/2}$ orbitals. For all the calculations the transition probabilities ($B(M1)$ and $B(E2)$) have been calculated

TABLE II: Lifetimes of the states in ^{29}Si from the present work in comparison to the previously reported values. The quoted uncertainties include the effect of the uncertainties in the stopping powers. Please refer to the text for details.

J_i^π	E_x	E_γ	τ (fs)	
			Present Work	NNDC
	(keV)	(keV)		
$3/2_1^+$	1274	1274	444^{+39}_{-53}	420^{+14}_{-14}
$5/2_1^+$	2028	2028	444^{+44}_{-40}	442^{+14}_{-14}
$5/2_2^+$	3067	1793	$< 28^{+3\,a}_{-3}$	48^{+1}_{-1}
$7/2_1^-$	3624	1596	2541^{+226}_{-190}	3795^{+130}_{-130}
$7/2_1^+$	4080	2806	$< 155^{+27\,a}_{-10}$	63^{+17}_{-17}
$9/2_1^+$	4741	2713	$< 116^{+20\,a}_{-18}$	52^{+10}_{-10}
$(9/2_1^-)$	5255	1631	$< 169^{+24\,a}_{-28}$	118^{+6}_{-6}
$11/2_1^-$	6781	1526	$< 35^{+5\,a}_{-7}$	22^{+3}_{-3}
$9/2_2^-$	7340[b]	3716	$< 3^{+1\,a}_{-1}$	
	8642	3901	$< 32^{+12\,a}_{-13}$	< 20
$13/2_1^-$	8761	3506	$< 40^{+12\,a}_{-10}$	27^{+6}_{-6}

[a]The presence of a dominant side-feeding allowed for assignment of only an upper limit on the lifetime.

[b]New level, first observed in the present work.

TABLE III: Comparison of experimental and shell model calculated level energies and lifetimes in ^{29}Si. The states with lifetimes (or limits) measured in the present work have been marked in bold font.

Experimental			Shell Model Calculation			
			USDA		SDPFMW	
E_x	J^π	τ	E_x	τ	E_x	τ
(keV)		(fs)	(keV)	(fs)	(keV)	(fs)
1274	$3/2_1^+$	$\mathbf{444^{+39}_{-53}}$	**1252**	**574**	**1394**	**829**
2028	$5/2_1^+$	$\mathbf{444^{+44}_{-40}}$	**2062**	**297**	**2123**	**282**
2427	$3/2_2^+$	26^{+1}_{-1}	2578	12	2633	13
3067	$5/2_2^+$	$\mathbf{48^{+1}_{-1}}$	**3256**	**24**	**3516**	**21**
4080	$7/2_1^+$	$\mathbf{63^{+17}_{-17}}$	**4219**	**43**	**4412**	**46**
4741	$9/2_1^+$	$\mathbf{52^{+10}_{-10}}$	**4593**	**81**	**4780**	**65**
5286	$7/2_2^+$	9^{+4}_{-4}	5128	11	5221	9
5652	$9/2_2^+$	74^{+4}_{-4}	5486	77	5783	64
6424	$(7/2_3^+)$	<20	5942	32	5881	16
6615	$(9/2_3^+)$	<20	6795	34	6991	33
7139	$(11/2_1^+)$	42^{+14}_{-14}	7049	42	7307	40
8173	$(11/2_2^+)$	<20	7967	13	8120	13
3624	$7/2_1^-$	$\mathbf{2541^{+226}_{-190}}$			**3485**	
5255	$\mathbf{(9/2_1^-)}$	$\mathbf{118^{+6}_{-6}}$			**5159**	**83**
6781	$11/2_1^-$	$\mathbf{22^{+3}_{-3}}$			**6546**	**34**
7340	$9/2_2^-$	$\mathbf{<3^{+1}_{-1}}$			**8788**	**12**
8761	$13/2_1^-$	$\mathbf{27^{+6}_{-6}}$			**8383**	**21**

using the effective g-factors and the effective charges from Ref. [8] ($g_{lp} = 1.175, g_{sp} = 5.000, g_{tp} = 0.260, g_{ln} = -0.106, g_{sn} = -3.500, g_{tn} = -0.170, e_p = 1.36, e_n = 0.45$). The specific features and results of these calculations are described in the subsequent sections.

A. Calculations for ^{29}Si

The positive parity states in the ^{29}Si nucleus have been calculated using both the $USDA$ and the $SDPFMW$ interactions with only the sd model space considered in both cases. The results for ^{29}Si are presented in Tables III and IV. The level energies and the lifetimes for the positive parity states from the calculations are in reasonable agreement with the experimental values (Table III). The negative parity states in this nucleus have been calculated for the first time in the present work, using $1\hbar\omega$ excitations. The results exhibit satisfactory conformity with the present measurements.

The $B(M1)$ and $B(E2)$ values of the transitions for which the branching ratios could be determined in the present investigation, have also been compared with the shell model calculations (Table IV) and found to be in adequate concurrence.

The ^{29}Si nucleus, being a mid-shell system, is expected to manifest deformation characteristics [27]. The deformation characteristics of the nucleus can be probed from the shell model calculations, through the quadrupole moments determined using the following equations [31].

$$Q = Q_0 \frac{3K^2 - J(J+1)}{(J+1)(2J+3)} \tag{3}$$

and,

$$B(E2 : J_i \rightarrow J_f) = \frac{5}{16\pi} e^2 Q_0^2 < J_i K 20 | J_f K >^2 \tag{4}$$

where Q and Q_0 are respectively the spectroscopic and the intrinsic quadrupole moments.

For the sequence of levels $E_x(J^\pi) = 3624$ $(7/2^-)$, 5255 $(9/2^-)$, 6781 $(11/2^-)$, the calculations indicate an

TABLE IV: Comparison of the experimental transition probabilities and branching ratios of the ^{29}Si nucleus, wherever possible, with those from the shell model calculations.

			Experimental			Shell Model					
E_x	E_γ	M				USDA			SDPFMW		
(keV)	(keV)		B(M1) (μ_n^2)	B(E2) (e^2fm^4)	BR	B(M1) (μ_n^2)	B(E2) (e^2fm^4)	BR	B(M1) (μ_n^2)	B(E2) (e^2fm^4)	BR
1274	1274	M1+E2	$0.06^{+0.01}_{-0.01}$	$19.08^{+2.58}_{-1.54}$	1.00	0.05	28.36	1.00	0.02	34.81	1.00
2028	2028	E2		$49.29^{+5.42}_{-4.07}$	0.92±0.01		64.09	0.87		63.31	0.94
3067	1793	M1+E2	$0.16^{+0.01}_{-0.01}$	$48.21^{+2.09}_{-1.93}$	0.83±0.01	0.21	71.90	0.82	0.21	58.16	0.80
4080	2806	E2		$49.88^{+18.43}_{-10.59}$	0.67±0.18		43.76	0.54		53.10	0.74
	2052	M1+E2	$0.03^{+0.01}_{-0.01}$	$0.72^{+0.27}_{-0.15}$	0.32±0.10	0.05	0.60	0.40	0.02	2.68	0.23
4741	2713	E2		$99.29^{+23.64}_{-16.02}$	0.93±0.07		94.06	0.98		93.88	0.99
5255	1631	(M1+E2)	$0.09^{+0.01}_{-0.01}$	$93.49^{+5.05}_{-4.52}$	1.00				0.12	157.10	1.00
6781	1526	M1+E2	$0.30^{+0.05}_{-0.04}$	$166.54^{+26.30}_{-19.98}$	0.45±0.17				0.28	143.90	0.48
	3157	E2		$63.86^{+10.08}_{-7.66}$	0.54±0.28					46.02	0.52

oblate deformation at the lowest spin, represented by $Q \sim$ -30 efm^2 and $Q_0 \sim$ -63 mb, evolving to a prolate deformation, with $Q \sim 2$ efm^2 ($Q_0 \sim 217$ mb), at $J^\pi = 11/2^-$. In particular, it may be noted that calculated $|Q_0| = 68$ fm^2, for the state $J^\pi = 9/2^-$ of this sequence, is in excellent overlap with the results of Bardin *et al.* [27] ($|Q_0| = 66 \pm 9$ fm^2). It is interesting that the present calculations corroborate the transitional characteristics of the ^{29}Si nucleus. This may imply an accurate inclusion of most of the dominant multi-particle configurations along with the appropriate two-body matrix elements herein. The previous studies have reported a considerably higher B(E2) value ($\sim$ 100-200 e^{2}fm^4) particularly for the aforesaid negative parity sequence which is also reproduced by the present calculations (Table IV). This may be construed as an indication for the onset of deformation in this nucleus. The success of the shell model approach in reproducing these deformation characteristics in ^{29}Si provided the motivation in exploring the strongly deformed structures, identified in the neighbouring ^{28}Si isotope in a similar perspective.

B. Deformation characteristics in ^{28}Si

In a recent study on ^{28}Si, Jenkins *et al.* [20] have confirmed the deformed structures in the nucleus and have proposed a candidate superdeformed band in the same. Antisymmetrized Molecular Dynamics (AMD) calculations [32] have been found to corroborate the experimental observations. Calculations have been carried out in the present work to explore the possibility of interpreting the aforesaid bands in the ^{28}Si nucleus within the shell model framework. The positive parity states, reported to be constituting these deformed bands, have been calculated using the $USDA$ and the $SDPFMW$ interactions. In case of the latter, only $0\hbar\omega$ excitations have been considered.

The results of the calculations for the ^{28}Si nucleus are presented in Table V. The level excitation energies from the measurements have been well represented in these calculations. The experimental $B(E2)$ values for the intra-band $E2$ transitions have been determined, based on inputs from the NNDC database [23] and compared with the calculations. For the ground state oblate band, the experimental trend of increasing $B(E2)$ followed by a reduction is well reproduced by the calculations. Further, the transition strengths (in Wu) for the oblate (ground state), the prolate (normal deformed) and the candidate for the superdeformed (SD) band in ^{28}Si, as identified by Jenkins *et al.* [20], have been computed and compared in Fig. 8. As seen from the figure, most of the transition probabilities are in qualitative agreement with the experimental results. The deviations in the higher spin states may warrant further experimental and computational investigations. The quadrupole moments for the oblate ground state band and the prolate (normal deformed) bands have also been calculated using Equations (3) and (4) and presented in Table VI. The values for the quadrupole moments uphold the oblate as-

TABLE V: The shell model calculations for the bands identified in the ^{28}Si nucleus [20], compared to the available experimental results.

		Experimental				Shell Model							
						USDA				*SDPFMW*			
Band	J^π	E_{expt} (keV)	E_γ (keV)	τ_N (fs)	$B(E2)$ e^2fm^4	E_{SM} (keV)	τ (fs)	B(E2) e^2fm^4	Q efm^2	E_{SM} (keV)	τ (fs)	B(E2) e^2fm^4	Q efm^2
Oblate	2_1^+	1779	1779	685±24	$66.85^{+2.43}_{-2.26}$	1940	355	83.56	19.09	1990	320	81.85	18.78
	4_1^+	4618	2839	53±6	$83.48^{+10.66}_{-8.49}$	4549	58	116.90	23.05	4659	52	115.80	23.25
	6_1^+	8544	3926	16±1	$54.68^{+3.64}_{-3.22}$	8395	10	98.75	28.65	8457	10	100.60	28.69
	8_1^+	14642	6098			14305	2	66.49	25.56	14212	2	73.42	26.82
SD	2_8^+	9796	3106			10693	6	2.12	-8.56	10688	7	1.81	-9.66
			8018					2.03				1.51	
	4_7^+	10946	2687	22±14		11481	39	9.47	10.87	11550	15	0.92	3.55
			3530					0.23				1.40	
			3565					0.15	10.87			0.18	
			9167					0.00				0.39	
	6_6^+	12865	1919			13423	6	3.84	12.46	13591	8	0.50	10.21
			3700					0.00				0.04	
			5977					9.07				4.83	
			8247					0.18				0.01	
Prolate	0_3^+	6691	4912	212±14	$1.34^{+0.10}_{-0.08}$	7478	85	1.83	0.00	7235	46	4.51	0.00
	2_2^+	7381	5602	7±3		7524	8	14.31	-10.28	7521	12	11.38	-7.36
			7381		$1.91^{+1.44}_{-0.57}$			0.94				0.29	
	4_3^+	9165	1749	40±4	$62.32^{+6.92}_{-5.67}$	9369	49	63.15	-4.71	9489	68	65.56	-9.54
			1784		$158.05^{+17.56}_{-14.37}$			1.17				0.03	
			4547					1.61				2.31	
			7386		$0.44^{+0.05}_{-0.04}$			0.47				0.15	
	6_4^+	11509	2344	13±3	$186.29^{+55.88}_{-34.93}$	11953	16	30.37	8.67	11815	16	43.06	0.99
			4621		$17.27^{+5.19}_{-3.24}$			16.67				17.15	
			6891		$0.84^{+0.25}_{-0.16}$			0.09				0.24	
vibr.	0_2^+	4979	3200	50±3	$48.63^{+3.11}_{-2.75}$	4821	58	70.12	0.00	5013	47	69.04	0.00
	2_5^+	8259	3280	14±3	$30.70^{+8.38}_{-5.42}$	8860	24	20.81	0.32	8665	14	1.89	9.37
			6480		$4.13^{+1.12}_{-0.72}$			0.46				0.01	
(K=3^+)	3_1^+	6277	1659	1125±86		6460	2324	10.27	11.57	6163	5475	6.66	13.99
			4498					0.00				0.00	
	4_2^+	6888	5109	48±3	$4.88^{+0.32}_{-0.29}$	7069	23	9.76	4.74	7032	30	8.22	4.99
	5_1^+	8945	2057	84±9		9302	42	88.15	2.43	9227	56	85.74	4.07
			4327					5.87				5.11	
	6_3^+	11331	6713	<30	< 1.99	11531	91	0.00	6.56	11508	42	0.38	13.48
	7_2^+	13710	5166			14352	13	0.12	12.70	14374	8	0.00	8.67

signment for the former while a change of deformation is indicated at the highest spin in case of the prolate band. It is further interesting to note that, for the (proposed) SD band, the current calculations result in a moment of inertia value in the range 5-9 $\hbar^2/MeV$, similar to the values reported in the recent study by Jenkins *et al.* [20].

C. Re-examining shell model calculations in ^{30}Si

Based on the success of the shell model calculations in reproducing the general deformation characteristics in the ^{28}Si nucleus, we have extended these calculations to the next higher even-even Si isotope, ^{30}Si. Such an extension is of significance because the $N \sim 20$ nuclei [1, 2, 4, 7] have been investigated, both experimentally and theoretically, with specific motivation to explore the effects of intruder states from the *fp* shells on their

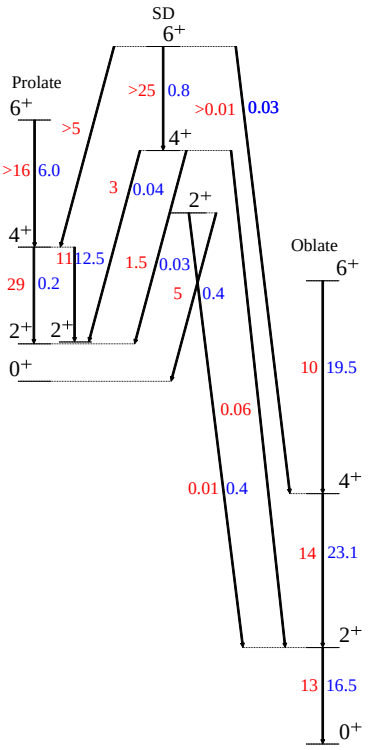

FIG. 8: (Color online) Comparison of the $B(E2)$ transition probabilities (in Wu), in ^{28}Si, as reported by Jenkins *et al.* [20] with those from the present calculations (blue for $USDA$).

TABLE VI: Static intrinsic quadrupole moment of the ground state oblate band and the excited prolate (normal deformed) band in ^{28}Si from the present shell model calculations (using $USDA$ interaction).

Band	J^π	Q (Theo.) (efm^2)	Q_0 [a] (mb)	B(E2) (Theo.) (e^2fm^4)	$\|Q_0\|$ [b] (mb)
Oblate	2^+	19.09	-668	83.56	648
	4^+	23.05	-634	116.90	641
	6^+	28.65	-716	98.75	562
	8^+	25.56	-607	66.49	450
Prolate	2^+	-10.28	360	-	
	4^+	-4.71	130	1.17	64
	6^+	8.67	-217	30.37	312

[a] Calculated using Equation (3)
[b] Calculated using Equation (4)

level structure. It is expected that these configurations would dominate the level structures at much lower excitation energies than the general expectation. Several factors could contribute to such a significant drop in the excitation energies of these intruder orbitals. The main contribution could arise from the many body correlations, which tend to lower the shell gaps.

Several studies on the *sdpf* nuclei have attempted to explain the observed level structures by introducing a nucleus specific reduction [21, 22] in the single particle energies of the intruder levels, and have attributed the agreement of such (shell model) calculations with the deduced level structure as a signature of the reduced shell gaps. However, it may be noted that these calculations have been performed using a large model space and consequently, a truncation scheme had to be introduced owing to the computational limitations. It has been well established that an inadequate truncation of the model space renders the ground state less bound [30], resulting in the predicted excitation energies being substantially higher. Further, a crucial ingredient of such calculations is the choice of appropriate two-body matrix elements. The success of the present shell model calculations for ^{28,29}Si validates the use of the model space and the choice of two-body matrix elements which motivated us to undertake the shell model calculations for ^{30}Si in an analogous way.

Previously, the shell model calculations for the ^{30}Si nucleus have been carried out by Steppenbeck *et al.* [7] using the USD, $USDA$ and $USDB$ interactions for the positive parity states and the WBP and the $WBP-a$ interactions for the negative parity states. They reported a satisfactory reproduction of the positive parity states in these calculations. The predictions for the negative parity states with WBP interaction had to be shifted down by ~ 2 MeV relative to the ground state. The calculated negative parity states, with the $WBP-a$ interaction, were equally or more discrepant with respect to the data and was ascribed to the inappropriate adjustments to the single particle energies of the $0f_{7/2}$ and $1p_{3/2}$ orbitals.

In the present work, calculations have been carried out for the positive and the negative parity levels of the ^{30}Si nucleus. The $SDPFMW$ interaction has been used for the purpose. The positive parity states have been have been calculated using the full *sd* model space and $0\hbar\omega$ excitation while the the negative parity states have been calculated using the *sdpf* model space with $1\hbar\omega$ excitations. The results are presented in Fig 9. The present calculations reproduce the experimental results satisfactorily. The compliance with the experimental data, particularly for the negative parity states, is substantially improved with respect to the previous studies. It is worthwhile to mention that there has been no reduction of the bare single particle energies for the $f_{7/2}$ and $p_{3/2}$ orbitals in the present work. Such

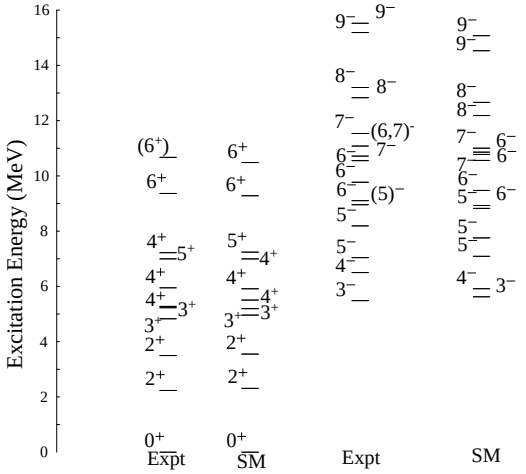

FIG. 9: Comparison of experimental level energies of the ^{30}Si nucleus from Ref. [7] with the shell model calculations in the present work. These calculations for ^{30}Si have been carried out using the $SDPFMW$ interaction with purely *sd* configurations for the positive parity states and $1\hbar\omega$ excitations for the negative parity states.

adjustments, as mentioned before, have been reported by Steppenbeck *et al.* [7] in their calculations of ^{30}Si nucleus with $WBP-a$ interaction.

The present work establishes the possibility to interpret the observed level sequences along with the deformation characteristics in the *sdpf* nuclei, within the shell model framework through proper choice of the effective interactions and the associated model space.

V. CONCLUSION

The ^{29}Si nucleus has been studied through heavy-ion induced fusion-evaporation reaction and, for the first time, using a large array of Compton suppressed Clover detectors. The existing level structure for the nucleus has been confirmed, on the basis of energy, anisotropy and polarization measurements, and a new level has been identified at $E_x = 7340$ keV, de-exciting by a 3716 keV γ-transition. Level lifetimes have been extracted using DSAM, with appropriate modifications of the analysis programmes to suit the thick molecular target used in the present setup. Most of the previously reported lifetimes have been reproduced in the present study, either directly or through an upper limit. However, the lifetime of the $E_x = 3624$ keV state, de-exciting by 1596 keV transition, has been determined to be 2.541^{+226}_{-190} ps at substantial variance with reported value of 3.795 ± 0.130 ps. This transition is of mixed E1+M2 nature, connecting the lowest negative parity state to the lower lying deformed states. It is interesting to note that a similar transition exists in the neighbouring ^{31}Si isotope, albeit with an enhanced B(E1) value which might indicate an enhancement of collectivity with increasing neutron number in the Si isotopes. Large basis shell model calculations have been carried out for the nucleus and the results are in satisfactory agreement with the experimental findings, including the deformation characteristics.

In view of the success of the calculations for the ^{29}Si nucleus, these have been extended to the neighbouring ^{28}Si and ^{30}Si isotopes. The deformation features in the former have been well represented in the present calculations. The calculations in case of the ^{30}Si nucleus have been carried out without any ad hoc lowering of the single particle energies, contrary to the previous studies, and the experimental level energies, both for the positive and the negative parity states, have been satisfactorily reproduced.

The present investigation has thus established the feasibility of implementing shell model calculations for interpretation of the level sequences in these transitional nuclei and the deformation features therein. Appropriate truncation schemes and choice of effective interactions, however, remain the crucial inputs for such an exercise.

ACKNOWLEDGMENT

The authors thank all the participants of the INGA collaboration for their help in setting up the facility at IUAC, New Delhi and TIFR, Mumbai. We are thankful to J. P. Greene (ANL, USA) for the ^{18}O target. The authors appreciate the help and support from Mr. Kausik Basu (UGC-DAE CSR, KC), Mr. B. S. Naidu, and Mr. S. Jadhav (TIFR) during the experiments. The authors also thank the Pelletron staff at IUAC, New Delhi and TIFR, Mumbai for their excellent support during the experiments. Discussions with Prof. Alex Brown on the shell model calculations have been of great help and are deeply appreciated. SSB would like to acknowledge the financial assistance in the form of a fellowship (SRF, CSIR sanction No. 09/838(0038)2010-EMR-I) from the Council of Scientific and Industrial Research (CSIR), Government of India. The INGA Project is partially supported by the Department of Science Technology (DST), Government of India, under Grant No. IR/S2/PF-03/2003-III. This work has been supported in part by the U.S. National Science Foundation (Grants No. PHY-1068192 and PHY-1419765).

[1] R. Chakrabarti, S. Mukhopadhyay, Krishichayan, A. Chakraborty, A. Ghosh, S. Ray, S. S. Ghugre, A. K. Sinha, L. Chaturvedi, A. Y. Deo, et al., Phys. Rev. C **80**, 034326 (2009).

[2] R. Chakrabarti, S. Mukhopadhyay, R. Bhattacharjee, S. S. Ghugre, A. K. Sinha, A. Dhal, L. Chaturvedi, M. K. Raju, N. Madhavan, R. P. Singh, et al., Phys. Rev. C **84**, 054325 (2011).

[3] S. S. Bhattacharjee, R. Bhattacharjee, R. Chakrabarti, R. Raut, S. S. Ghugre, A. K. Sinha, T. Trivedi, L. Chaturvedi, S. Saha, J. Sethi, et al., Phys. Rev. C **89**, 024324 (2014).

[4] P. C. Bender, C. R. Hoffman, M. Wiedeking, J. M. Allmond, L. A. Bernstein, J. T. Burke, D. L. Bleuel, R. M. Clark, P. Fallon, B. L. Goldblum, et al., Phys. Rev. C **80**, 014302 (2009).

[5] G. Neyens, Phys. Rev. C **84**, 064310 (2011).

[6] J. R. Terry, B. A. Brown, C. M. Campbell, J. M. Cook, A. D. Davies, D. C. Dinca, A. Gade, T. Glasmacher, P. G. Hansen, B. M. Sherrill, et al., Phys. Rev. C **77**, 014316 (2008).

[7] D. Steppenbeck, A. Deacon, S. Freeman, R. Janssens, M. Carpenter, C. Hoffman, B. Kay, T. Lauritsen, C. Lister, D. ODonnell, et al., Nucl. Phys. A **847**, 149 (2010).

[8] W. A. Richter, S. Mkhlze, and B. A. Brown, Phys. Rev. C **78**, 064302 (2008).

[9] R. Bhattacharjee, S. S. Bhattacharjee, K. Basu, P. V. Rajesh, R. Raut, S. S. Ghugre, D. Das, A. K. Sinha, L. Chaturvedi, U. Garg, et al., Phys. Rev. C **90**, 044319 (2014).

[10] D. C. Bailey, P. E. Carr, J. L. Durell, L. L. Green, M. W. Green, A. N. James, J. F. Sharpey-Schaffer, and D. A. Viggars, J. Phys. A **5**, 596 (1972).

[11] S. I. Baker and R. E. Segel, Phys. Rev. **170**, 1046 (1968).

[12] P. R. Dekock, J. W. Koen, and W. L. Mouton, Nucl. Phys. A **140**, 190 (1970).

[13] T. R. Fisher, T. T. Bardin, J. A. Baker, and A. D. W. Jones, Bull. Am. Phys. Soc **15**, 600 (1970).

[14] E. C. Booth and K. A. Wright, Nucl. Phys. **35**, 472 (1962).

[15] T. W. Retz-Schimdt, S. J. Skorka, H. Morgenstern, and H. Schimdt, C. R. Congr. Intern. Phys. Nucl. **2**, 396 (1964).

[16] D. E. C. Scherpenzeel, G. A. P. Engelbertink, H. J. M. Aarts, C. J. V. D. Poel, and H. F. R. Arciszewski, Nucl. Phys. A **349**, 513 (1980).

[17] P. Tikkanen, J. Keinonen, A. Kuronen, A. Z. Kiss, E. Koltay, E. Pintye, and B. H. Wildenthal, Nucl. Phys. A **517**, 176 (1990).

[18] J. M. J. Wozniak, R. L. Hershberger, and D. J. Donahue, Phys. Rev. **181**, 1580 (1969).

[19] J. A. Becker, L. F. Chase, and R. E. McDonald, Phys. Rev. **157**, 967 (1967).

[20] D. G. Jenkins, C. J. Lister, M. P. Carpenter, P. Chowdury, N. J. Hammond, R. V. F. Janssens, T. L. Khoo, T. Lauritsen, D. Seweryniak, T. Davidson, et al., Phys. Rev. C **86**, 064308 (2012).

[21] P. Mason, N. Marginean, S. N. Lenzi, M. Ionescu-Bujor, F. D. Vedova, D. R. Napoli, T. Otsuka, Y. Utsuno, F. Nowacki, M. Axiotis, et al., Phys. Rev. C **71**, 014316 (2005).

[22] M. Ionescu-Bujor, A. Iordachescu, D. R. Napoli, S. N. Lenzi, N. Marginean, T. Otsuka, Y. Utsuno, R. V. Ribas, M. Axiotis, D. Bazzacco, et al., Phys. Rev. C **73**, 024310 (2005).

[23] URL `www.nndc.bnl.gov`.

[24] J. C. Wells and N. R. Johnson, ORNL Report **6689**, 44 (1991).

[25] URL `www.srim.org`.

[26] A. Gavron, Phys. Rev. C **21**, 230 (1980).

[27] T. T. Bardin, J. A. Becker, T. R. Fisher, and A. D. W. Jones, Phys. Rev. Lett. **24**, 772 (1970).

[28] T. T. Bardin, J. A. Becker, T. R. Fisher, and A. D. W. Jones, Phys. Rev. C **4**, 1625 (1971).

[29] B. A. Brown and W. D. M. Rae, MSU-NSCL Report (2007).

[30] E. K. Warburton, J. A. Becker, and B. A. Brown, Phys. Rev. C **41**, 1147 (1990).

[31] R. F. Casten, *Nuclear Structure from a Simple Perspective, Second Edition* (Oxford Science Publications, 1999).

[32] Y. Taniguchi, Y. Kanada-Eńyo, and M. Kimura, Phys. Rev. C **80**, 059903 (2009).